

NASA TM X-838

NASA

RESEARCH ADMINISTRATION

DECLASSIFIED- US: 1688  
TAINÉ TO ROBERTSON MEMO  
DATED 9/28/66

## TECHNICAL MEMORANDUM

X-838

Declassified by authority of NASA  
Classification Change Notices No. 90  
Dated \*\* 10/12/66

LONGITUDINAL AERODYNAMIC CHARACTERISTICS AT  
MACH NUMBER 2.02 OF A SERIES OF WING-BODY CONFIGURATIONS  
EMPLOYING A CAMBERED AND TWISTED ARROW WING

By Harry W. Carlson

Langley Research Center  
Langley Station, Hampton, Va.

GPO PRICE \$ \_\_\_\_\_

CFSTI PRICE(S) \$ \_\_\_\_\_

Hard copy (HC) 1.00Microfiche (MF) .50

FACILITY FORM 602

N66 39608

(ACCESSION NUMBER)

19

(PAGES)

TMX-838

(NASA CR OR TMX OR AD NUMBER)

(THRU)

(CODE)

0

(CATEGORY)

4 553 JULY 65

NATIONAL AERONAUTICS AND SPACE ADMINISTRATION  
WASHINGTON

July 1963

TECHNICAL MEMORANDUM X-838

LONGITUDINAL AERODYNAMIC CHARACTERISTICS AT  
 MACH NUMBER 2.02 OF A SERIES OF WING-BODY CONFIGURATIONS  
 EMPLOYING A CAMBERED AND TWISTED ARROW WING\*

By Harry W. Carlson

SUMMARY

An investigation of the longitudinal aerodynamic characteristics of wing-body configurations employing a twisted and cambered,  $70^\circ$  swept arrow wing of aspect ratio 2.24 was performed in the Langley 4- by 4-foot supersonic pressure tunnel at a Mach number of 2.02 and a Reynolds number of  $4.4 \times 10^6$  based on the mean aerodynamic chord. Each of the seven configurations tested had the same distribution of normal cross-sectional areas but had different body center-line incidence and camber. The best aerodynamic performance of the test models was obtained with a body cambered so that its thickness was added symmetrically above and below the wing camber surface. This result suggests a simple design procedure for treating the addition of a fuselage to a warped wing so as to preserve the benefits of twist and camber. The improvement in maximum lift-drag ratio (7.9 compared with a value of 6.8 for the corresponding flat wing configuration) was near the theoretical increment with leading-edge suction effects neglected. The experimental lift-drag ratio, however, fell far short of that theoretically attainable with full leading-edge suction.

INTRODUCTION

Previous wind-tunnel force and pressure tests of a series of arrow wings (refs. 1 and 2) have shown significant improvements in maximum lift-drag ratio through the use of twist and camber. The greatest improvement (an increase in maximum lift-drag ratio from 8.1 to 8.8) was shown, in reference 1, for a wing designed for a lift coefficient of 0.08, which was approximately one-half that required for the maximum lift-drag ratio.

The tests reported herein were performed to investigate the longitudinal aerodynamic characteristics of wing-body combinations employing the above-mentioned best wing from the tests of reference 1, the purpose of this study being to help establish design methods for employing twist and camber to the

\*Title, Unclassified.

Declassified by authority of NASA  
 Classification Change Notices No. 20  
 Dated 10/12/66

~~CONFIDENTIAL~~

best advantage in complete configurations. Each of the seven configurations studied had the same distribution of normal cross-sectional areas but had different body center-line incidence and camber. The investigation was conducted in the Langley 4- by 4-foot supersonic pressure tunnel at a Mach number of 2.02 and a Reynolds number of  $4.4 \times 10^6$  based on the mean aerodynamic chord.

# SYMBOLS

$b/2$	wing semispan
$c$	local wing chord
$\bar{c}$	wing mean aerodynamic chord
$C_A$	axial-force coefficient, $\frac{\text{Axial force}}{qS}$
$C_D$	drag coefficient, $\frac{\text{Drag}}{qS}$
$C_L$	lift coefficient, $\frac{\text{Lift}}{qS}$
$C_m$	pitching-moment coefficient about $\bar{c}/4$ , $\frac{\text{Pitching moment}}{qS\bar{c}}$
$L/D$	lift-drag ratio, $C_L/C_D$
$q$	free-stream dynamic pressure
$r$	body radius
$S$	wing area
$t$	wing thickness
$x, y, z$	Cartesian coordinate system in which X-axis is intersection of wing horizontal reference plane and wing-body vertical plane of symmetry, origin at or directly above or below body nose
$x'$	distance from wing leading edge measured in x-direction
$\alpha$	angle of attack

# REPORT

## MODELS AND INSTRUMENTATION

A photograph of a representative model is shown in figure 1 and drawings of the test wing-body configurations are presented in figures 2 and 3. A layout of the wing planform and basic body is shown in figure 2 along with tabulated values of the wing camber surface, the wing thickness, and the body radius. The wings employed are a reference flat wing, designated as wing 1, and a twisted and cambered wing with a design lift coefficient of 0.08, designated as wing 2. These 70° swept wings of aspect ratio 2.24 are identical to wings of the same designations in references 1 and 2. Figure 3 illustrates the body camber and incidence with respect to the wing reference plane used in the seven test configurations. Also presented in figure 3 are the tabulated ordinates of the body center line.

The reference wing-body, configuration 1, employs a wing with no twist and camber and the basic body with no incidence or camber. Configuration 2 employs the cambered wing with the basic uncambered body aligned with the free stream when the wing is at design attitude ( $C_L = 0.08$ ). For configuration 3 the body is aligned with the wing root chord. Configuration 4 is similar to configuration 3 except for the "upswept" afterbody. Configuration 5 has the upswept afterbody and also has a modified nose section. The body center line for both the nose and afterbody sections is aligned with the free stream when the wing is at design condition. In a sense, configuration 5 has the body thickness added symmetrically above and below the wing camber surface. Configurations 6 and 7 are similar to configuration 5 (mid-wing) except that the body surface is coincident with the wing lower surface for configuration 6 (low-wing) and is coincident with the upper surface for configuration 7 (high-wing).

The bodies were attached to the half-span steel wings, which in turn were mounted on a four-component strain-gage balance housed within a boundary-layer bypass plate. During the tests, the wing and plate moved through an angle-of-attack range as a unit. A clearance of 0.010 to 0.020 inch was provided between the body and the surface of the plate. Tests of one of these models with increasing gap between model and plate showed no measurable effect on the forces until clearances significantly greater than 0.020 inch were used.

## TESTS

The tests were conducted in the Langley 4- by 4-foot supersonic pressure tunnel at a free-stream Mach number of 2.02 and a Reynolds number of  $4.4 \times 10^6$  based on the mean aerodynamic chord. In order to insure a turbulent boundary layer, transition strips were used on all wing-body combinations. For the wings, a 1/8-inch-wide strip of No. 80 carborundum grains in a lacquer binder was placed 1/4 inch behind the wing leading edge. For the bodies, No. 60 carborundum grains were used in a 1/8-inch-wide strip 1 inch behind the nose.

Angle of attack was measured optically with the use of prisms recessed in the wing surface.

~~CONFIDENTIAL~~

From pretest calibrations and repeatability of the data, the aerodynamic coefficients are estimated to be accurate within the following limits:

$C_D$	.....	$\pm 0.0003$
$C_L$	.....	$\pm 0.0030$
$C_m$	.....	$\pm 0.0010$

## RESULTS AND DISCUSSION

The aerodynamic characteristics in pitch of the seven configurations are given as a function of lift coefficient in figure 4. The data are presented for groups of three configurations for ease in making comparisons.


In figure 4(a) a comparison may be made between the basic wing-body (configuration 1) and configurations employing the basic uncambered body at two incidence angles on the twisted and cambered wing. Configuration 3, using a body aligned with the wing root chord of the twisted and cambered wing, is seen to provide a sizable improvement in maximum lift-drag ratio compared with that of the basic wing-body combination.

Figure 4(b) shows the effect of nose and afterbody modifications to configuration 3. A slightly greater maximum lift-drag ratio with some decrease in pitching moment at zero lift is shown for configuration 5. This configuration, which produced the highest maximum lift-drag ratio of these tests, employs a body whose thickness may be said to have been added symmetrically above and below the camber surface. At the design condition ( $C_L = 0.08$ ), the body center line basically follows a path along the free-stream direction from the body nose to the wing apex, then along the root chord to the wing trailing edge, and leaves the wing in the free-stream direction.

A comparison of the high-, mid-, and low-wing configurations is shown in figure 4(c). The mid-wing configuration, as stated previously, provided the highest maximum lift-drag ratio and the low-wing configuration provided the next highest value.

Theoretical estimates are compared with measured aerodynamic data in figure 5. Drag due to lift at design condition was found by an integration over the wing planform of the specified load distribution (ref. 1) and the required camber surface slopes as defined by the methods of reference 3. Drag due to lift at other lift coefficients was found by applying an increment due to flat-plate loading on this planform by using the equations of reference 4. Thickness drag for the wing-body combination was found by using area-rule concepts and the evaluation methods suggested in reference 5.

In figure 5, data are shown for the best of the combined wing-body combinations (configuration 5) and for the uncambered wing-body (configuration 1). There is reasonable agreement between experiment and theory. The improvement in maximum lift-drag ratio (7.9 for configuration 5 compared with a value of 6.8 for

  
configuration 1) is near the theoretical increment with leading-edge suction effects neglected. However, the maximum experimental lift-drag ratio falls far short of the theoretical value attainable with full leading-edge suction.

The increase in lift-drag ratio due to twist and camber for the wing alone is compared with the increase for the best of the wing-body combinations in figure 6. It is interesting to note that a greater portion of the theoretical improvement in  $L/D$  is attained for the wing-body combination than for the wing alone.

#### CONCLUDING REMARKS

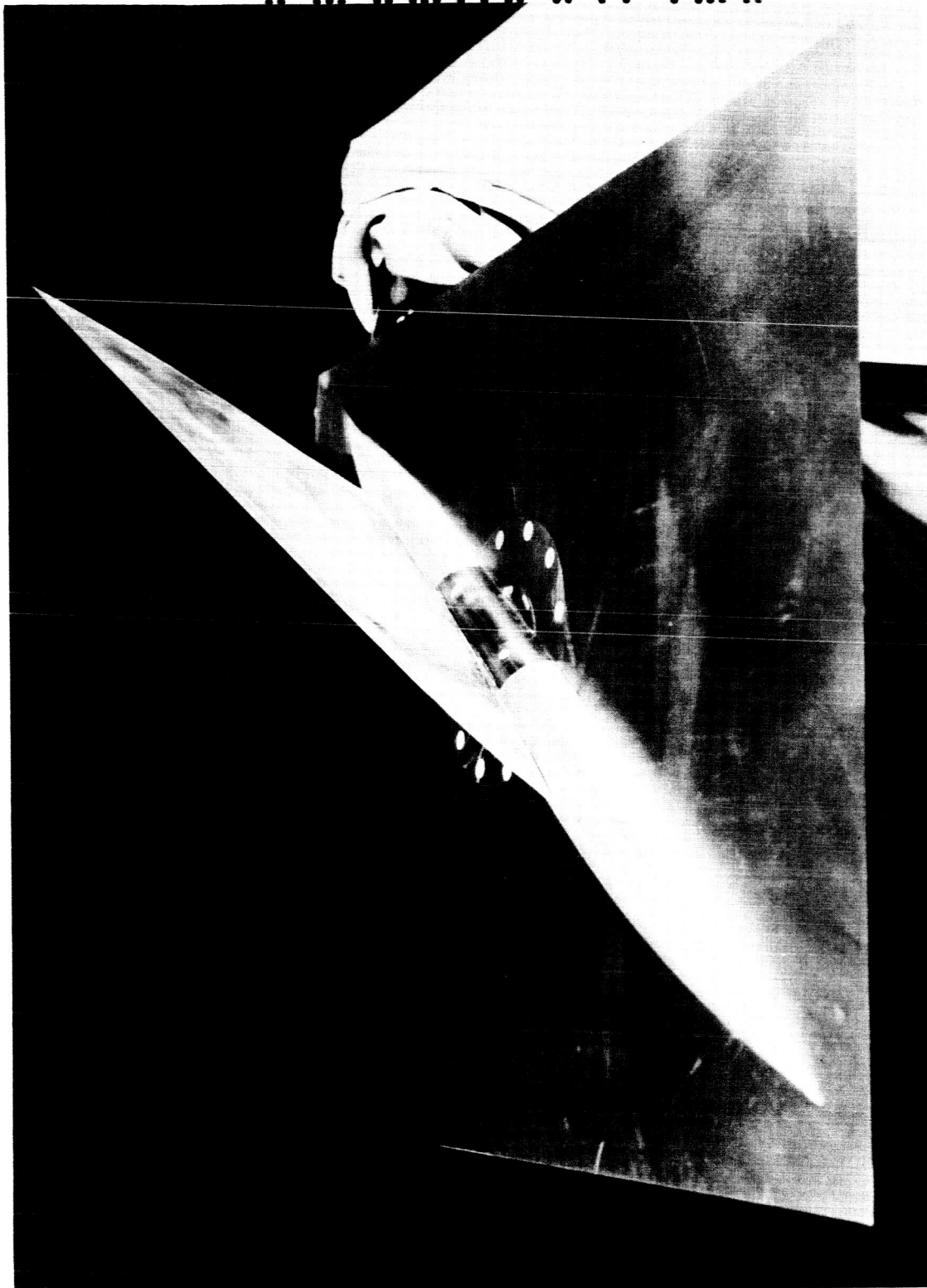
An experimental study of the longitudinal aerodynamic characteristics of wing-body configurations employing a twisted and cambered wing indicated that the best performance of the test models was obtained with a body cambered so that its thickness was added symmetrically above and below the wing camber surface. This result suggests a simple design procedure for treating the addition of a fuselage to a warped wing so as to preserve the benefits of twist and camber. The improvement in maximum lift-drag ratio (7.9 compared with a value of 6.8 for the corresponding "flat" configuration) is near the theoretical increment with leading-edge suction effects neglected. The experimental lift-drag ratio, however, falls far short of that theoretically attainable with full leading-edge suction.

Langley Research Center,  
National Aeronautics and Space Administration,  
Langley Station, Hampton, Va., May 8, 1963.

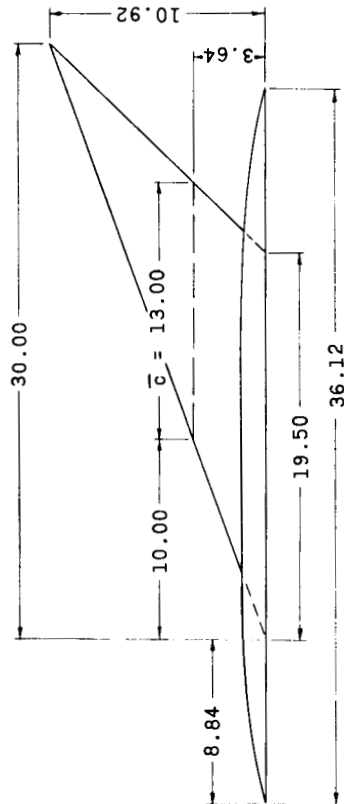
~~CONFIDENTIAL~~  
REFERENCES

1. Carlson, Harry W.: Aerodynamic Characteristics at Mach Number 2.05 of a Series of Highly Swept Arrow Wings Employing Various Degrees of Twist and Camber. NASA TM X-332, 1960.
2. Carlson, Harry W.: Pressure Distributions at Mach Number 2.05 on a Series of Highly Swept Arrow Wings Employing Various Degrees of Twist and Camber. NASA TN D-1264, 1962.
3. Tucker, Warren A.: A Method for the Design of Sweptback Wings Warped To Produce Specified Flight Characteristics at Supersonic Speeds. NACA Rep. 1226, 1955. (Supersedes NACA RM L51F08.)
4. Brown, Clinton E.: Theoretical Lift and Drag of Thin Triangular Wings at Supersonic Speeds. NACA Rep. 839, 1946. (Supersedes NACA TN-1183.)
5. Emlinton, E., and Lord, W. T.: Note on the Numerical Evaluation of the Wave Drag of Smooth Slender Bodies Using Optimum Area Distributions for Minimum Wave Drag. Jour. R.A.S., vol. 60, no. 541, Jan. 1956, pp. 61-63.

REF ID: A66057



L-62-9745  
Figure 1.- Photograph of representative model mounted on boundary-layer bypass plate.



Wing 1  
 $C_{L,design} = 0$

Wing sections at  $\frac{y}{b/2} = .30$

Wing 2  
 $C_{L,design} = .08$

Wing-camber surface ordinates,  $\frac{z}{C_{L,design}}$

$\frac{y}{b/2}$	0	.025	.050	.100	.200	.300	.400	.500	.600	.700	.800	.900	1.00
0	12.00	11.60	11.10	10.10	8.20	6.06	3.30	1.14	-0.31	-2.34	-5.40	-7.92	-10.00
.1	4.70	4.76	4.76	4.60	3.70	2.61	1.29	.12	-1.60	-3.00	-4.30	-5.63	-6.89
.2	1.65	1.74	1.86	1.86	1.44	.81	.0	.12	-.84	-1.70	-2.72	-3.66	-4.05
.3	.31	.67	.77	.87	.69	.33	.12	.66	-1.30	-1.95	-2.63	-3.29	-3.05
.4	.68	.80	.90	1.06	1.11	.96	.44	.56	-.31	-.72	-1.24	-1.84	-1.84
.5	.84	.96	1.05	1.20	1.37	1.35	1.20	1.00	.75	.45	.12	.24	.64
.6	.98	1.10	1.20	1.36	1.56	1.62	1.56	1.50	1.36	1.12	.82	.50	.50
.7	1.14	1.26	1.34	1.50	1.70	1.80	1.86	1.83	1.60	1.71	1.62	1.50	1.30
.8	1.30	1.43	1.46	1.60	1.77	1.92	2.00	2.04	2.06	2.06	2.04	2.00	1.86
.9	1.44	1.49	1.52	1.60	1.72	1.83	1.94	2.01	2.07	2.13	2.18	2.21	2.23
1.0	1.60												

Wing thickness,  $t$  (3 per cent circular-arc sections)

$\frac{y}{b/2}$	0	.025	.050	.100	.200	.300	.400	.500	.600	.700	.800	.900	1.00
0	0	.056	.112	.212	.376	.492	.562	.586	.562	.492	.376	.212	0
.1	0	.050	.101	.190	.338	.442	.506	.527	.506	.442	.338	.190	0
.2	0	.045	.090	.169	.300	.393	.449	.468	.449	.393	.300	.169	0
.3	0	.039	.078	.147	.262	.344	.393	.410	.393	.344	.262	.147	0
.4	0	.034	.067	.127	.225	.295	.337	.351	.337	.295	.225	.127	0
.5	0	.028	.056	.105	.187	.246	.281	.293	.281	.246	.187	.105	0
.6	0	.022	.045	.085	.150	.196	.225	.234	.225	.196	.150	.085	0
.7	0	.017	.034	.063	.112	.147	.168	.176	.168	.147	.112	.063	0
.8	0	.011	.022	.042	.075	.098	.112	.117	.112	.098	.075	.042	0
.9	0	.006	.011	.021	.037	.049	.056	.059	.056	.049	.037	.021	0
1.0	0	0	0	0	0	0	0	0	0	0	0	0	0

Basic-body radius,  $r$

$\frac{y}{b/2}$	0	.025	.050	.100	.200	.300	.400	.500	.600	.700	.800	.900	1.00
0	0	0	0	0	0	0	0	0	0	0	0	0	0
.1	0	0	0	0	0	0	0	0	0	0	0	0	0
.2	0	0	0	0	0	0	0	0	0	0	0	0	0
.3	0	0	0	0	0	0	0	0	0	0	0	0	0
.4	0	0	0	0	0	0	0	0	0	0	0	0	0
.5	0	0	0	0	0	0	0	0	0	0	0	0	0
.6	0	0	0	0	0	0	0	0	0	0	0	0	0
.7	0	0	0	0	0	0	0	0	0	0	0	0	0
.8	0	0	0	0	0	0	0	0	0	0	0	0	0
.9	0	0	0	0	0	0	0	0	0	0	0	0	0
1.0	0	0	0	0	0	0	0	0	0	0	0	0	0

$\frac{y}{b/2}$	0	.025	.050	.100	.200	.300	.400	.500	.600	.700	.800	.900	1.00
0	0	0	0	0	0	0	0	0	0	0	0	0	0
.1	0	0	0	0	0	0	0	0	0	0	0	0	0
.2	0	0	0	0	0	0	0	0	0	0	0	0	0
.3	0	0	0	0	0	0	0	0	0	0	0	0	0
.4	0	0	0	0	0	0	0	0	0	0	0	0	0
.5	0	0	0	0	0	0	0	0	0	0	0	0	0
.6	0	0	0	0	0	0	0	0	0	0	0	0	0
.7	0	0	0	0	0	0	0	0	0	0	0	0	0
.8	0	0	0	0	0	0	0	0	0	0	0	0	0
.9	0	0	0	0	0	0	0	0	0	0	0	0	0
1.0	0	0	0	0	0	0	0	0	0	0	0	0	0

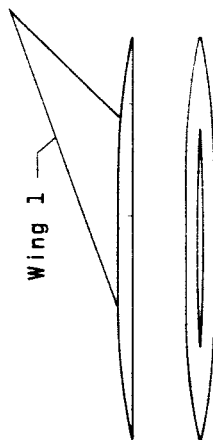
$\frac{y}{b/2}$	0	.025	.050	.100	.200	.300	.400	.500	.600	.700	.800	.900	1.00
0	0	0	0	0	0	0	0	0	0	0	0	0	0
.1	0	0	0	0	0	0	0	0	0	0	0	0	0
.2	0	0	0	0	0	0	0	0	0	0	0	0	0
.3	0	0	0	0	0	0	0	0	0	0	0	0	0
.4	0	0	0	0	0	0	0	0	0	0	0	0	0
.5	0	0	0	0	0	0	0	0	0	0	0	0	0
.6	0	0	0	0	0	0	0	0	0	0	0	0	0
.7	0	0	0	0	0	0	0	0	0	0	0	0	0
.8	0	0	0	0	0	0	0	0	0	0	0	0	0
.9	0	0	0	0	0	0	0	0	0	0	0	0	0
1.0	0	0	0	0	0	0	0	0	0	0	0	0	0

$\frac{y}{b/2}$	0	.025	.050	.100	.200	.300	.400	.500	.600	.700	.800	.900	1.00
0	0	0	0	0	0	0	0	0	0	0	0	0	0
.1	0	0	0	0	0	0	0	0	0	0	0	0	0
.2	0	0	0	0	0	0	0	0	0	0	0	0	0
.3	0	0	0	0	0	0	0	0	0	0	0	0	0
.4	0	0	0	0	0	0	0	0	0	0	0	0	0
.5	0	0	0	0	0	0	0	0	0	0	0	0	0
.6	0	0	0	0	0	0	0	0	0	0	0	0	0
.7	0	0	0	0	0	0	0	0	0	0	0	0	0
.8	0	0	0	0	0	0	0	0	0	0	0	0	0
.9	0	0	0	0	0	0	0	0	0	0	0	0	0
1.0	0	0	0	0	0	0	0	0	0	0	0	0	0

Figure 2.- Typical planform of wing-body combinations and tabulated ordinates of wing camber surfaces, wing thickness distribution, and basic body thickness distribution. (All dimensions in inches.)

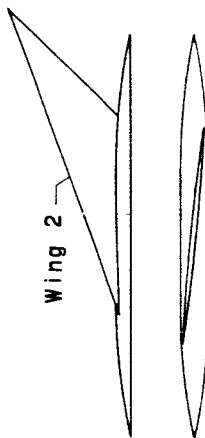
Body-camber ordinates, z

x	Configuration						
	1	2	3	4	5	6	7
0	0	0	1.72	1.72	0.96	2.15	-0.22
2	0	0	1.54	1.54	1.54	2.10	→
4	0	0	1.35	1.35	1.35	1.68	→
6	0	0	1.17	1.17	1.17	1.44	→
8	0	0	0.99	0.99	0.92	1.22	→
10	0	0	0.80	0.80	0.80	1.00	→
12	0	0	0.62	0.62	0.62	0.80	→
14	0	0	0.43	0.43	0.43	0.62	→
16	0	0	0.25	0.25	0.25	0.43	→
18	0	0	0.07	0.07	0.07	0.25	→
20	0	0	-0.11	-0.11	-0.11	0.07	→
22	0	0	-0.30	-0.30	-0.30	0.00	→
24	0	0	-0.48	-0.48	-0.48	0.00	→
26	0	0	-0.67	-0.67	-0.67	0.00	→
28	0	0	-0.85	-0.85	-0.85	0.00	→
30	0	0	-1.04	-1.04	-1.04	0.00	→
32	0	0	-1.22	-1.22	-1.22	0.00	→
34	0	0	-1.40	-1.40	-1.40	0.00	→
36	0	0	-1.58	-1.58	-1.58	0.00	→

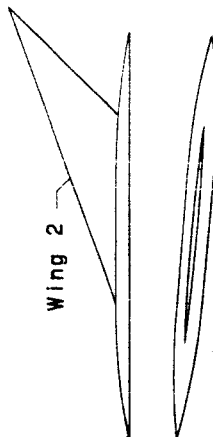


Configuration 1

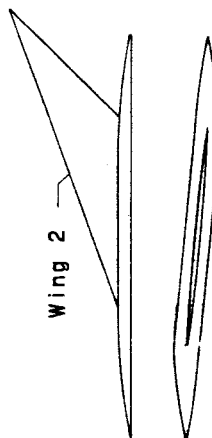
(no camber in wing or body)



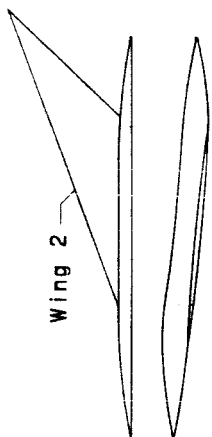
Configuration 2



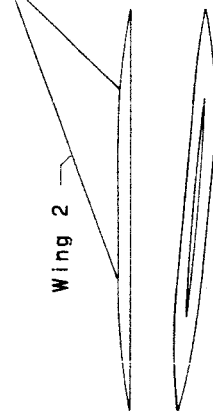
Configuration 3



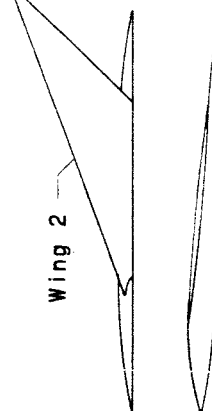
Configuration 5



Configuration 6

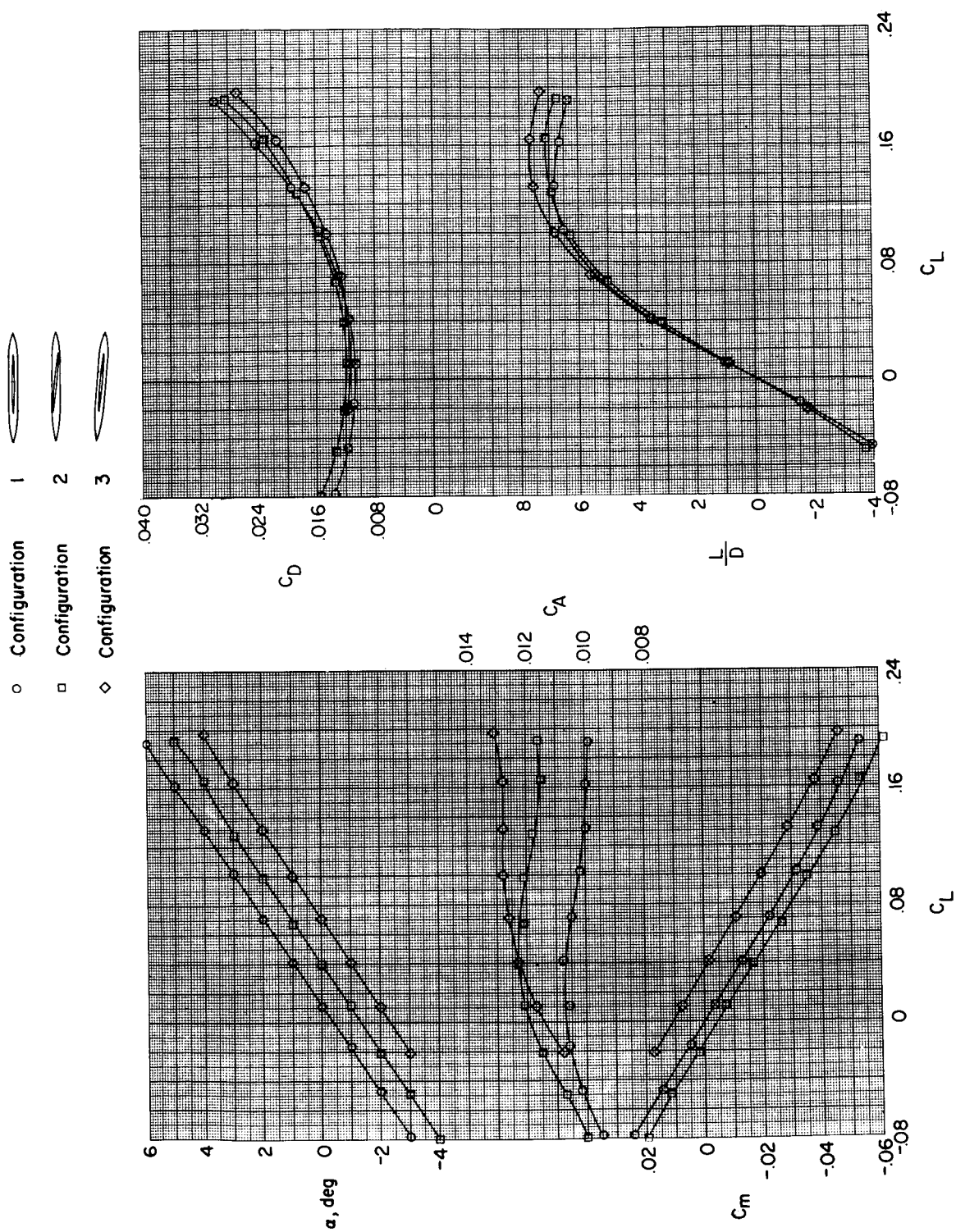


Configuration 4



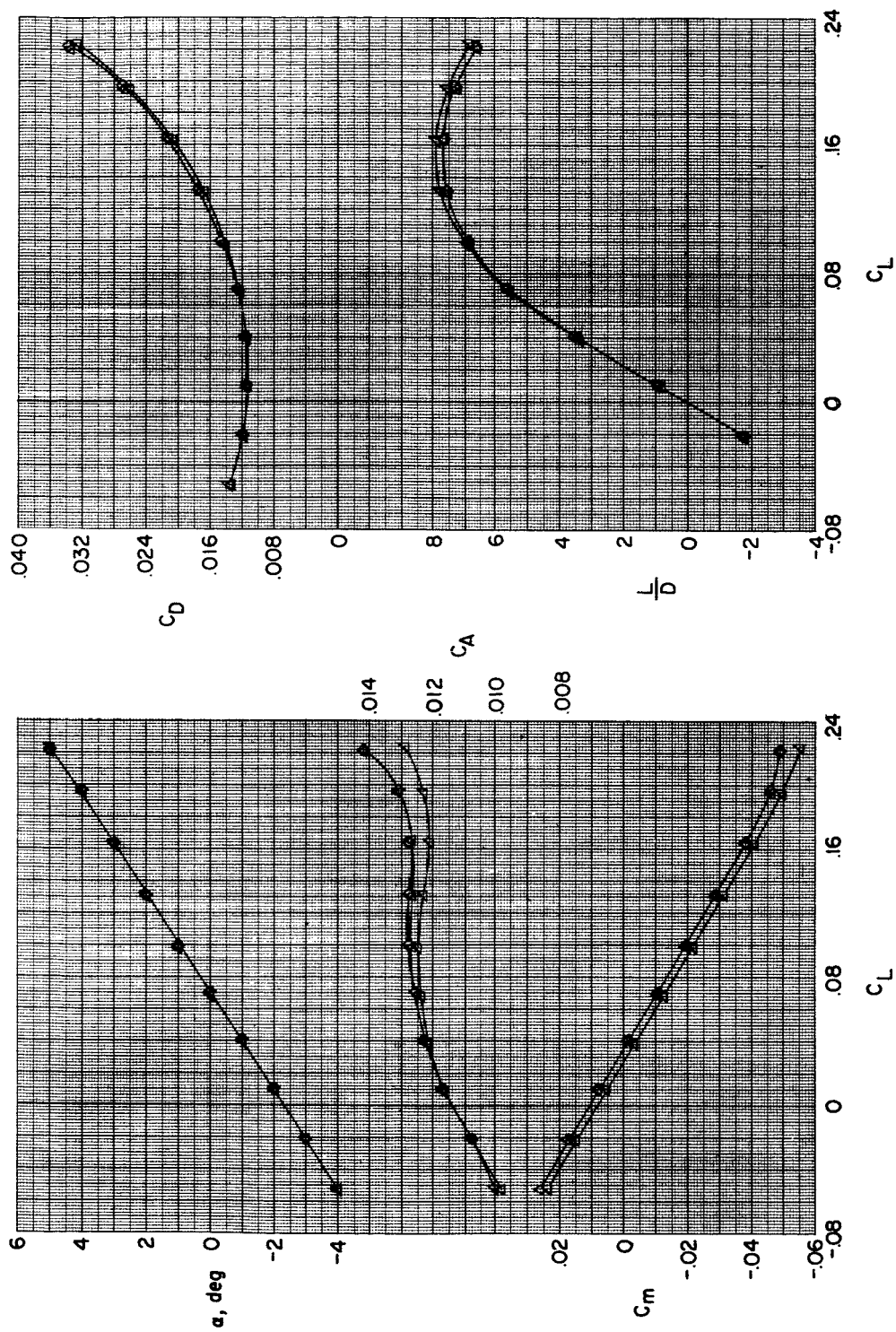
Configuration 7

Figure 3.- Sketches of wing-body combinations and tabulated ordinates of the body center-line camber.  
(All dimensions in inches.)



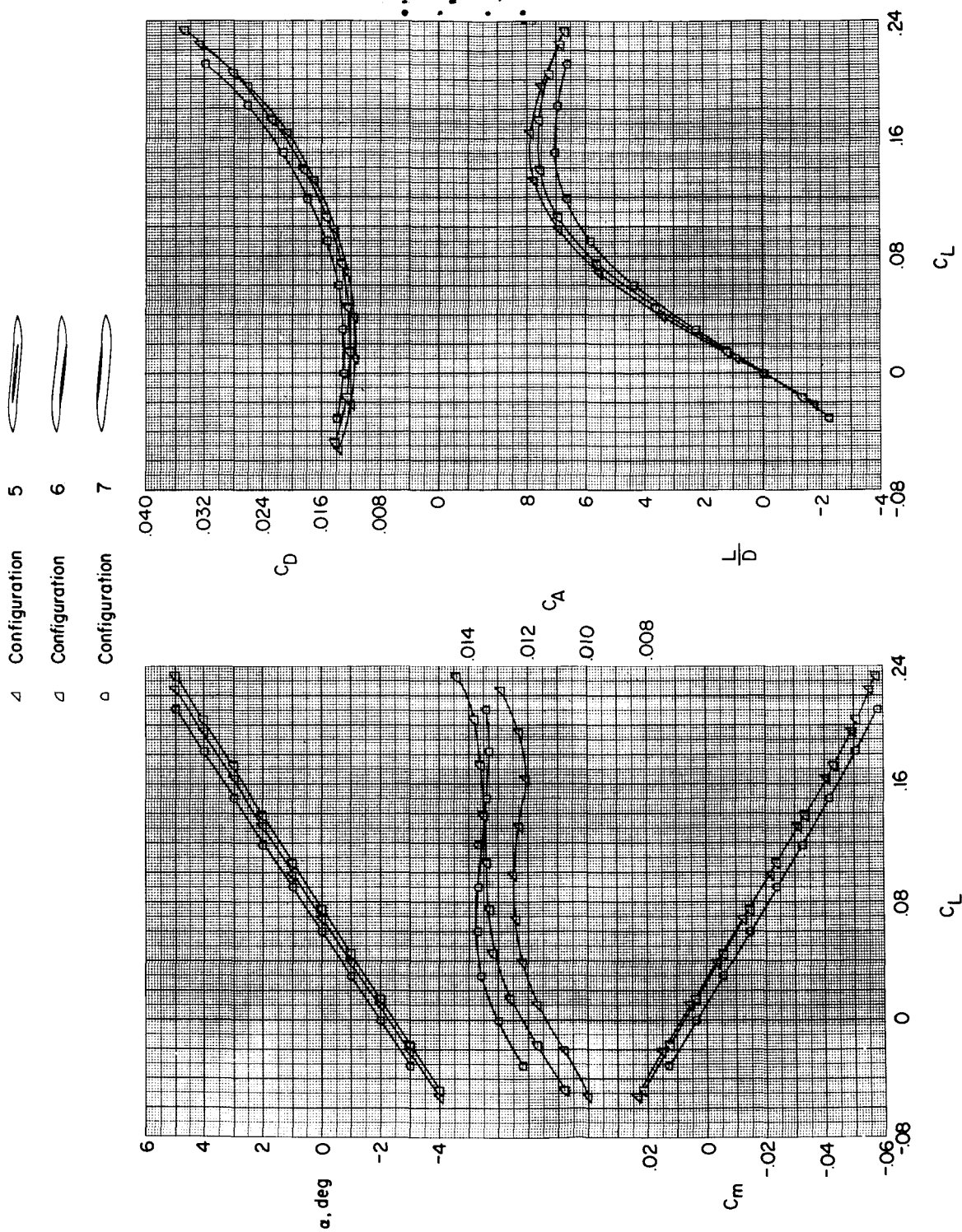
(a) Configurations 1, 2, and 3.

Figure 4.- Measured aerodynamic characteristics of the wing-body combinations.



(b) Configurations 3, 4, and 5.

Figure 4.- Continued.



(c) Configurations 5, 6, and 7.

Figure 4.- Concluded.

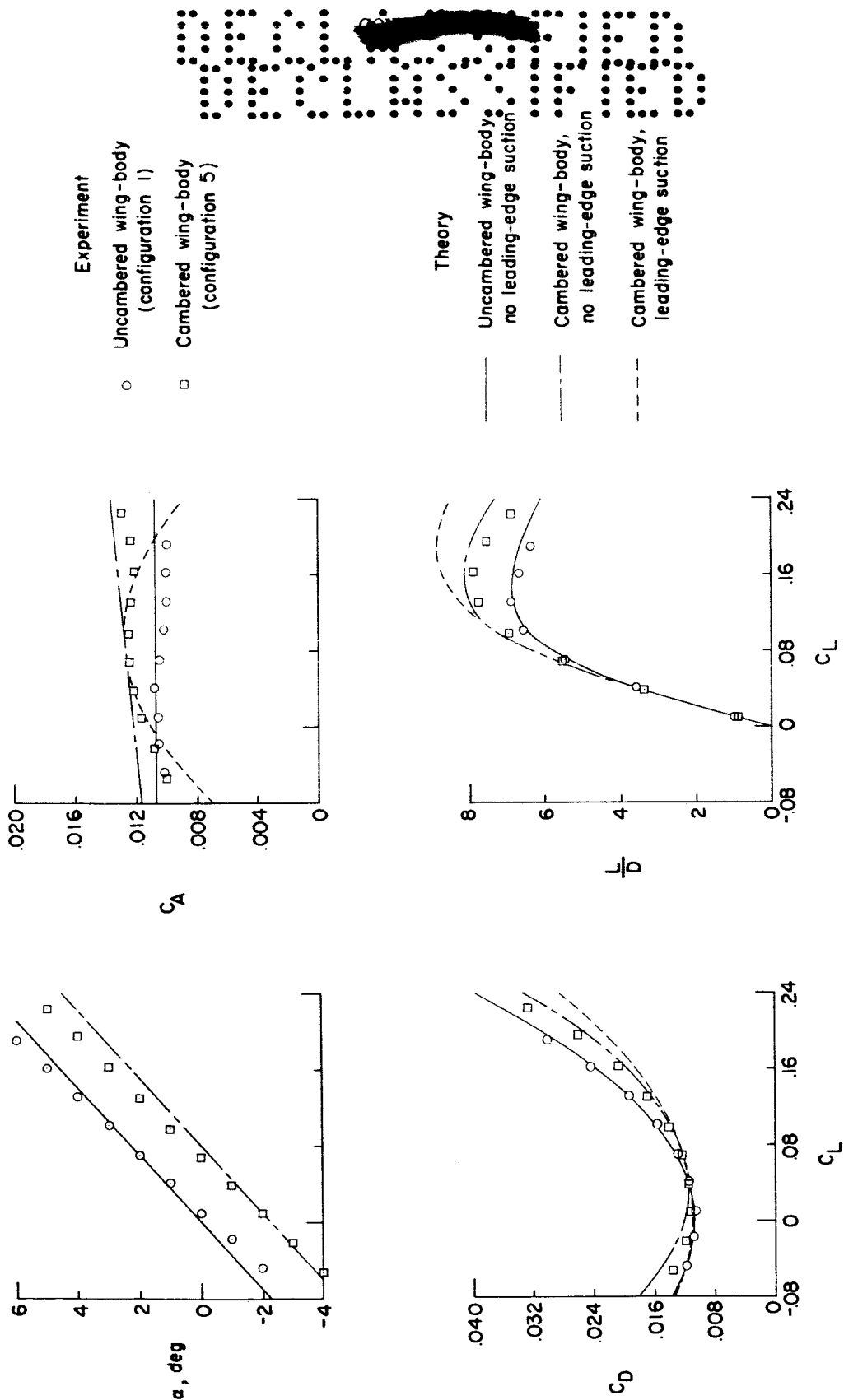


Figure 5.- Aerodynamic characteristics of the best of the cambered wing-body configurations compared with those of the corresponding uncambered configuration.

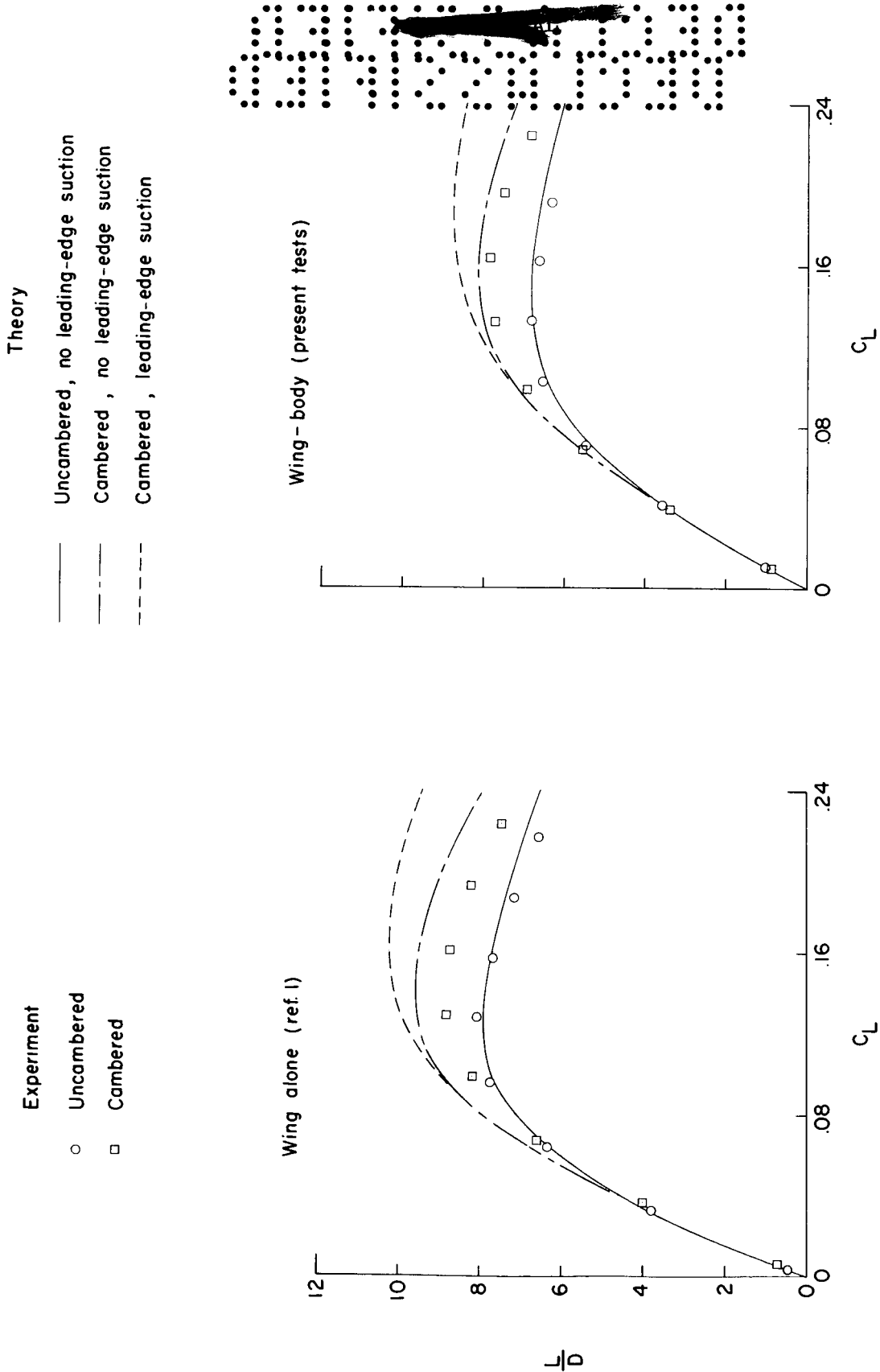


Figure 6.- Lift-drag ratios obtained with the cambered and uncambered wing-body combinations compared with lift-drag ratios for the cambered and uncambered wings alone.